

Crystal structure and magnetoresistance of $\text{La}_{(2-x)/3}\text{Nd}_{x/3}\text{Ca}_{1/3}\text{MnO}_3$: Local lattice distortion effect

G. H. Rao, J. R. Sun, J. K. Liang, and W. Y. Zhou

*Institute of Physics and Center for Condensed Matter Physics, Chinese Academy of Sciences, P.O. Box 603,
Beijing 100080, People's Republic of China*

(Received 15 May 1996; revised manuscript received 15 July 1996)

The crystal structure, low field ac susceptibility, magnetization, and magnetoresistance behavior of $\text{La}_{(2-x)/3}\text{Nd}_{x/3}\text{Ca}_{1/3}\text{MnO}_3$ ($x=0-2$) compounds are investigated. The crystal structure of the compounds belongs to an orthorhombically distorted perovskite structure. The lattice distortion and the bending of Mn-O-Mn bond increase with the increase of Nd content. ac susceptibility and magnetization measurements show that the magnetic transition temperature decreases with the increase of Nd content, and two evident magnetic transitions are observed for $x=0.75-1.0$. The magnetization isotherms exhibit a field-induced magnetic transition in the sample. Large magnetoresistance (MR) effects are observed in bulk $\text{La}_{(2-x)/3}\text{Nd}_{x/3}\text{Ca}_{1/3}\text{MnO}_3$ at low field. For bulk $\text{La}_{1/3}\text{Nd}_{1/3}\text{Ca}_{1/3}\text{MnO}_3$ a MR ratio as high as -96% is achieved in a field of 0.67 T. The maximum MR ratio in a field of 0.67 T increases linearly with the decrease of peak temperature of zero-field resistivity. Based upon the discussion on local distortions of the lattice and measurements of ac susceptibility, magnetization, and resistivity, a magnetic inhomogeneity model, i.e., simultaneous occurrence of metallic La-rich ferromagnetic domains and semiconducting Nd-rich domains, is proposed for the magnetic structure of $\text{La}_{(2-x)/3}\text{Nd}_{x/3}\text{Ca}_{1/3}\text{MnO}_3$ compounds. Within the framework of the magnetic inhomogeneity model, it is argued that the occurrence of resistivity peak could result from a competition of opposite temperature dependence of resistivities in La-rich phase and in Nd-rich phase, thus the peak temperature of resistivity does not necessarily correspond to a magnetic transition temperature. [S0163-1829(97)03206-2]

I. INTRODUCTION

Manganese perovskite $R_{1-x}A_x\text{MnO}_3$ (R =rare earth, A =alkaline earth) has attracted considerable attention recently owing to its giant magnetoresistance (GMR) effect that is considerably larger than the GMR observed in magnetic multilayers and alloys.¹⁻⁵ The parent antiferromagnetic insulator LaMnO_3 involves Mn^{3+} ions with $t_{2g}^3 e_g^1$ ($S=2$) configuration. The Hund-coupled t_{2g}^3 electrons may be viewed as a single local spin ($S=3/2$) because of their narrow one-electron bandwidth, while the e_g^1 state hybridized strongly with the $\text{O}2p$ states is either itinerant or localized. The parent compound LaMnO_3 is a Mott insulator due to the strong correlations of the e_g electrons.⁶ However, it was suggested that proper hole doping by substitution of divalent alkaline earth for R^{3+} ions in LaMnO_3 can lead to both metallic conductivity and ferromagnetism via a double exchange (DE) mechanism, i.e., the hopping of e_g electrons between Mn^{3+} and Mn^{4+} ions mediated by oxygen anions.⁷ The effective transfer integral of e_g electrons depends on the relative angle of the localized spins of manganese ions. The structure distortion may not only influence the effective transfer integral but also result in superexchange interaction between manganese ions and complicate the magnetic structure of the compound. Hwang *et al.*⁸ and Fonteberta *et al.*⁹ investigated the size effect of the ions at the A site in ABO_3 on the magnetoresistance of doped LaMnO_3 with fixed $\text{Mn}^{3+}/\text{Mn}^{4+}$ ratio and found that magnetic transition and significant magnetoresistance occurred at lower temperature as the average ionic radius at the A site was decreased. They argued that the bending of the Mn-O-Mn bond played

an important role for the size effect. The reported size effect is essentially an average effect. Different local distortion of the lattice around different ions could result in a magnetic inhomogeneity in the compound and give rise to an intriguing magnetic structure and magnetoresistance behavior.

In this paper, the crystal structure and magnetoresistance of $\text{La}_{(2-x)/3}\text{Nd}_{x/3}\text{Ca}_{1/3}\text{MnO}_3$ ($x=0-2$) are reported. The local distortions of the lattice around La^{3+} and Nd^{3+} ions are expected to be different, since, in addition to the difference in ionic radius, the end compound $\text{La}_{2/3}\text{Ca}_{1/3}\text{MnO}_3$ exhibited a magnetic ordering around 270 K with a fully spin-polarized magnetic moment,¹⁰ while the end compound $\text{Nd}_{2/3}\text{Ca}_{1/3}\text{MnO}_3$ showed a magnetic ordering around 100 K with a very low spontaneous magnetization at 77 K.¹¹ After a brief description of experimental procedure in Sec. II, the crystal structure, ac susceptibility, magnetization, and magnetoresistance of $\text{La}_{(2-x)/3}\text{Nd}_{x/3}\text{Ca}_{1/3}\text{MnO}_3$ compounds are reported in Sec. III. A possible relationship between lattice distortion and magnetic structure as well as magnetoresistance is discussed in Sec. IV, and finally a summary is given in Sec. V.

II. EXPERIMENTAL PROCEDURES

$\text{La}_{(2-x)/3}\text{Nd}_{x/3}\text{Ca}_{1/3}\text{MnO}_3$ ($x=0-2$) bulk samples were prepared by a standard ceramic processing route. Well mixed stoichiometric mixtures of La_2O_3 , Nd_2O_3 , MnO_2 and CaCO_3 were calcined at 1173 K for 24 h. The powder thus obtained was ground, pelletized, and sintered at 1373 K for 96 h with two intermediate grindings, then furnace cooled to room temperature. Phase purity and crystal structure of the synthesized samples were examined by x-ray powder diffraction.

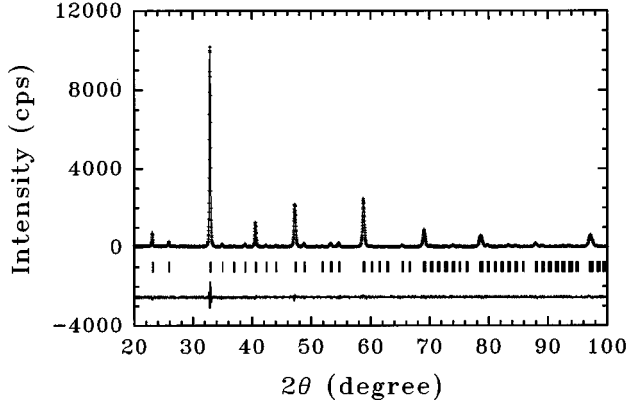


FIG. 1. XRD pattern of $\text{La}_{1/3}\text{Nd}_{1/3}\text{Ca}_{1/3}\text{MnO}_3$ compound. The observed data are indicated by crosses and the calculated profile is the continuous line overlying them. The lowest curve shows the difference between observed and calculated patterns. The vertical bars indicate the expected reflection positions.

tion, by using a Rigaku x-ray diffractometer with a rotating anode and CuK_α radiation.

Low field ac susceptibility of the samples between 77 K and 300 K was measured by means of a sensitive mutual inductance method with a frequency of 320 Hz. The magnetization of the samples was determined by an extracting sample magnetometer or a Quantum Design superconducting quantum interference device magnetometer. The resistance of the samples was measured by a standard four-probe method between 77 K and 300 K. The magnetoresistance (MR) ratio is defined here as $\Delta R/R = (R_H - R_0)/R_0$, where R_0 and R_H are resistances in a field of zero and H, respectively.

III. RESULTS

A. Crystal structure

X-ray powder diffraction (XRD) reveals that single-phase samples were obtained for $x = 0-2$. The diffraction peaks are

TABLE I. Final atomic parameters, weighted pattern R factor, “goodness of fit” (S) and selected Mn-O-Mn bond angle of $\text{La}_{(2-x)/3}\text{Nd}_{x/3}\text{Ca}_{1/3}\text{MnO}_3$ (space group $Pbnm$).

Composition	0.00	0.15	0.30	0.45	0.60	0.75	1.00	1.20	1.50	2.00
R (4c) x	0.4952(6)	0.4942(5)	0.4931(5)	0.4933(5)	0.4931(5)	0.4939(6)	0.4919(3)	0.4920(5)	0.4928(5)	0.4926(6)
y	0.0192(2)	0.0206(2)	0.0221(2)	0.0229(2)	0.0245(2)	0.0253(2)	0.0275(2)	0.0300(2)	0.0327(2)	0.0360(2)
z	0.25	0.25	0.25	0.25	0.25	0.25	0.25	0.25	0.25	0.25
Mn (4a) x	0.0	0.0	0.0	0.0	0.0	0.0	0.0	0.0	0.0	0.0
y	0.0	0.0	0.0	0.0	0.0	0.0	0.0	0.0	0.0	0.0
z	0.0	0.0	0.0	0.0	0.0	0.0	0.0	0.0	0.0	0.0
O1 (4c) x	0.5578(21)	0.5692(23)	0.5624(24)	0.5663(24)	0.5733(22)	0.5642(24)	0.5637(18)	0.5621(24)	0.5647(24)	0.5727(28)
y	0.4913(17)	0.4912(19)	0.4918(18)	0.4893(18)	0.4883(18)	0.4854(18)	0.4858(13)	0.4879(17)	0.4884(17)	0.4808(20)
z	0.25	0.25	0.25	0.25	0.25	0.25	0.25	0.25	0.25	0.25
O2 (8d) x	0.2217(19)	0.2234(22)	0.2220(21)	0.2241(24)	0.2238(22)	0.2215(22)	0.2182(16)	0.2243(22)	0.2220(22)	0.2157(24)
y	0.2726(22)	0.2766(23)	0.2754(23)	0.2788(21)	0.2817(19)	0.2790(22)	0.2819(15)	0.2864(19)	0.2854(20)	0.2846(22)
z	0.0287(11)	0.0254(13)	0.0297(12)	0.0252(13)	0.0254(12)	0.0311(12)	0.0294(10)	0.0346(12)	0.0374(11)	0.0361(17)
R_{wp} (%)	13.65	14.34	14.20	14.60	13.36	14.30	11.35	14.10	14.06	17.03
S	1.19	1.25	1.21	1.23	1.20	1.18	1.23	1.22	1.27	1.47
Mn-O1-Mn	161	158	160	159	156	159	159	160	159	156
Mn-O2-Mn	162	163	162	163	163	161	160	159	158	157

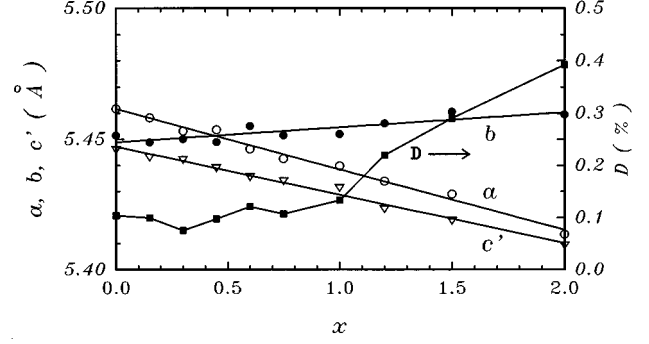


FIG. 2. Composition dependence of lattice constants and average distortion ratio of $\text{La}_{(2-x)/3}\text{Nd}_{x/3}\text{Ca}_{1/3}\text{MnO}_3$. $c' = c/\sqrt{2}$.

sharp and can be indexed by an orthorhombically distorted perovskite structure with space group $Pbnm$. The crystal structure was further refined by a standard Rietveld technique.¹² Figure 1 shows the observed and calculated XRD patterns of $\text{La}_{1/3}\text{Nd}_{1/3}\text{Ca}_{1/3}\text{MnO}_3$ compound. The final atomic parameters, weighted pattern R factor, “goodness of fit” (S),¹² and selected Mn-O-Mn bond angles of $\text{La}_{(2-x)/3}\text{Nd}_{x/3}\text{Ca}_{1/3}\text{MnO}_3$ are given in Table I. The structure refinement results are similar to those of $\text{Pr}_{1-x}\text{Ca}_x\text{MnO}_3$ series.¹³ Figure 2 shows the dependence of lattice constants on Nd content. The lattice constants a and c decrease linearly with the increase of Nd content, while b increases slightly. Although there is a crossover around $x=0.45$ from $a>b$ to $a<b$, $c/\sqrt{2}$ remains smaller than a and b over the whole composition range ($x=0-2$). Therefore, the crystal structure of $\text{La}_{(2-x)/3}\text{Nd}_{x/3}\text{Ca}_{1/3}\text{MnO}_3$ belongs to an O' -type structure,¹³ which is an orthorhombically distorted perovskite structure resulting from a cooperative Jahn-Teller effect of Mn^{3+} ions leading to distortions of Mn^{3+}O_6 octahedra and their cooperative ordering.

The deviation from cubic symmetry of an orthorhombic structure can be described by a so-called average distortion ratio, D , which is defined as¹³

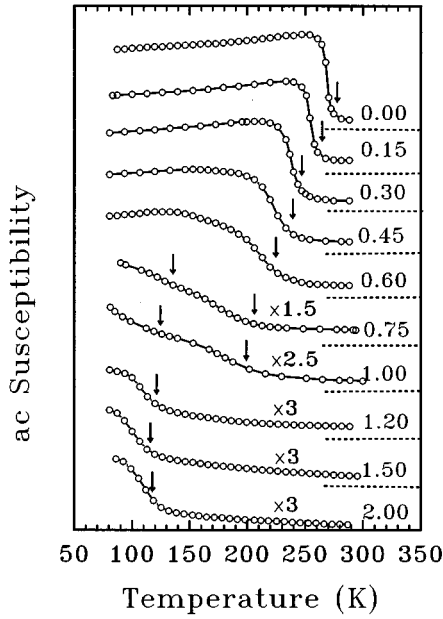


FIG. 3. Temperature dependence of low-field ac susceptibility of $\text{La}_{(2-x)/3}\text{Nd}_{x/3}\text{Ca}_{1/3}\text{MnO}_3$. The dotted lines are baselines for the corresponding curves and downward arrows indicate magnetic transition temperatures.

$$D = \frac{1}{3} \sum_{i=1}^3 \left| \frac{a_i - \bar{a}}{a_i} \right|,$$

where $\bar{a} = (abc/\sqrt{2})^{1/3}$, $a_1 = a$, $a_2 = b$, and $a_3 = c/\sqrt{2}$. The dependence of D on Nd content is also shown in Fig. 2. The average distortion ratio D exhibits a drastic increase around $x=1$ from $D \approx 0.1\%$ for $x < 1$ to $D \approx 0.39\%$ at $x=2$, which implies a larger orthorhombic distortion when $x > 1$. As shown in Table I, the angles of Mn-O-Mn bonds show a tendency to decrease with the increase of Nd content, i.e., the bending of Mn-O-Mn bonds increases with x .

B. ac susceptibility and magnetization

Low field ac susceptibility of $\text{La}_{(2-x)/3}\text{Nd}_{x/3}\text{Ca}_{1/3}\text{MnO}_3$ is shown in Fig. 3. For $x=0$, the susceptibility exhibits a sharp increase with the decrease of temperature, indicating an occurrence of magnetic ordering. The magnetic ordering corresponds to a paramagnetic-ferromagnetic transition at $T_m = T_c = 277$ K, which is consistent with previous reports.^{4,10} As the Nd content increases, T_m decreases and the width of the magnetic transition becomes more and more broad. For $x=0.75-1$, another magnetic transition occurring at low temperature is well developed, in addition to the one taking place at high temperature. When $x \geq 1.2$, however, the magnetic transition at high temperature is hardly observed, only the transition at low temperature can be determined, and the width of the magnetic transition becomes narrow again. For $x=2$, a magnetic transition takes place at $T_m = 118$ K, which agrees well with previous report.¹¹

Figure 4 shows the dependence of magnetic transition temperature on Nd content in $\text{La}_{(2-x)/3}\text{Nd}_{x/3}\text{Ca}_{1/3}\text{MnO}_3$. For $x=0.75-1$, two magnetic transition temperatures, T_m and $T_{m'}$, can be determined. T_m is coincident with the La-

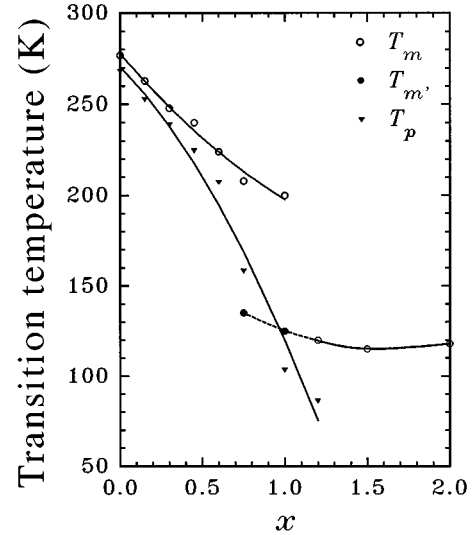


FIG. 4. Composition dependence of magnetic transition temperature and peak temperature of resistivity in zero field of $\text{La}_{(2-x)/3}\text{Nd}_{x/3}\text{Ca}_{1/3}\text{MnO}_3$. $T_{m'}$ is the second magnetic transition temperature for $x=0.75-1.0$. Solid lines are guides to the eyes.

rich branch of the T_m-x curve, while $T_{m'}$ coincident with the Nd-rich branch. It seems to indicate that the magnetic transition at high temperature is related to that in $\text{La}_{2/3}\text{Ca}_{1/3}\text{MnO}_3$, while the magnetic transition at low temperature is related to that in $\text{Nd}_{2/3}\text{Ca}_{1/3}\text{MnO}_3$.

Figure 5 presents the temperature dependence of magnetization of $\text{La}_{(2-x)/3}\text{Nd}_{x/3}\text{Ca}_{1/3}\text{MnO}_3$ with $x=0.75-1.2$. At a field of 0.5 T, the temperature dependence of magnetization is similar to that of low field ac susceptibility of the compound. Two magnetic transitions are evident for $x=0.75$ and 1.0. At a higher field of $H \geq 4$ T, the magnetization curve becomes a unified one, and the magnetization at low temperature corresponds to an almost fully spin-polarized state for the samples with $x=1.0$ and 1.2. The inset in Fig. 5 shows two magnetization isotherms at 100 K and

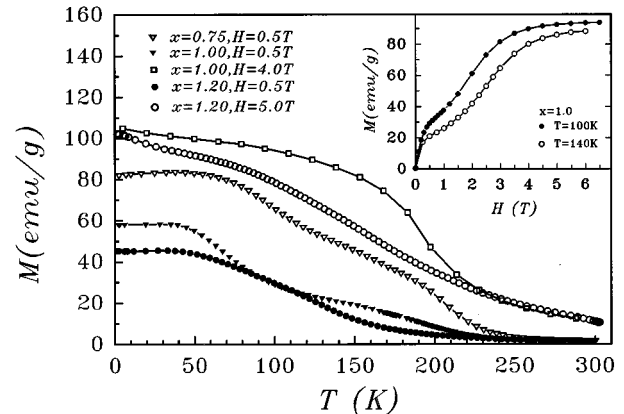


FIG. 5. Temperature dependence of magnetization of bulk $\text{La}_{(2-x)/3}\text{Nd}_{x/3}\text{Ca}_{1/3}\text{MnO}_3$ ($x=0.75-1.2$) measured in different magnetic fields. Field-cooling curves are shown. The inset shows the magnetization isotherms of the sample with $x=1.0$ at 100 and 140 K, respectively.

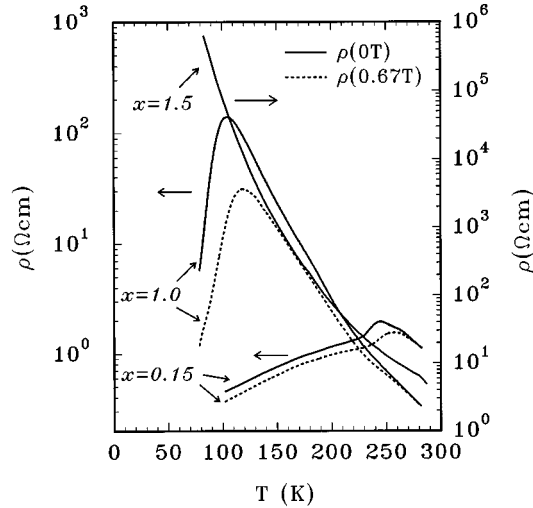


FIG. 6. Temperature dependence of resistivity of $\text{La}_{(2-x)/3}\text{Nd}_{x/3}\text{Ca}_{1/3}\text{MnO}_3$ for $x=0.3, 1.0,$ and $1.5,$ respectively. For $x=1.5,$ the difference between $\rho(0)$ and $\rho(0.67\text{ T})$ is very small.

140 K for the sample with $x=1.0$. Both the isotherms exhibit two plateaus: the lower one sets in at $H_1 \approx 0.5\text{ T}$, while the higher one, which corresponds to an almost fully spin-polarized state of the compound, sets in at $H_2 \approx 4\text{ T}$ and $H_2 \approx 4.5\text{ T}$ for the isotherms at 100 and 140 K, respectively. Between H_1 and H_2 , the magnetization shows a rapid increase at $H_c \approx 1.2\text{ T}$ and $H_c \approx 1.8\text{ T}$ for the isotherms at 100 and 140 K, respectively, indicating a field-induced magnetic transition.

C. Magnetoresistance

The magnetoresistance of the bulk $\text{La}_{(2-x)/3}\text{Nd}_{x/3}\text{Ca}_{1/3}\text{MnO}_3$ is measured by a standard four-probe method during cooling the sample from 300 to 77 K in zero field or in an applied field. In zero field, the resistivity exhibits a metallic behavior ($d\rho/dT > 0$) at low temperature and a semiconducting behavior ($d\rho/dT < 0$) at high temperature for $x \leq 1.2$. Figure 6 shows the temperature dependence of the resistivity of some samples. The sharp resistivity peak is indicative of the occurrence of metal-insulator ($M-I$) transition. The temperature corresponding to the resistivity peak T_p is also shown in Fig. 4. As the Nd content increases, T_p decreases rapidly and becomes more and more lower than the magnetic transition temperature, T_m .

When a magnetic field is applied, the temperature dependence of resistivity is similar to that in zero field, but the resistivity decreases, the resistivity peak broadens and shifts to a higher temperature. The direction of the applied field was the same as that of current. No obvious dependence on field orientation was observed if the demagnetization effect is taken into account. The largest change in resistivity takes place around the resistivity peak, and thus gives rise to a very prominent negative MR effect. For $\text{La}_{1/3}\text{Nd}_{1/3}\text{Ca}_{1/3}\text{MnO}_3$ bulk sample, a MR ration as high as -96% is achieved around $T \approx 90\text{ K}$ in a field of 0.67 T , which is the highest available magnetic field during cooling the sample in our experiment. Usually, the MR effect with

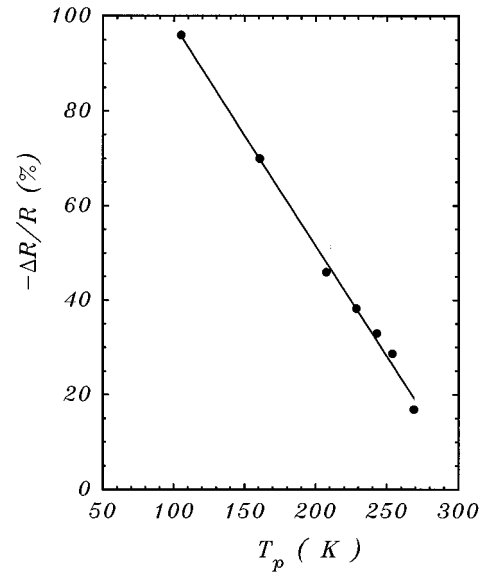


FIG. 7. Dependence of the maximum MR ratio in a field of 0.67 T on the peak temperature of resistivity in zero field.

$|\Delta R/R_0| > 90\%$ in $R_{1-x}A_x\text{MnO}_3$ was observed at much higher field ($6-12\text{ T}$).¹⁻⁵ In a field of 0.1 T , the MR ratio in bulk $\text{La}_{1/3}\text{Nd}_{1/3}\text{Ca}_{1/3}\text{MnO}_3$ is about -55% , which is much higher than the MR effect observed in the La-Ca-Mn-O film ($\sim -15\%$)¹ and in the La-Y-Ca-Mn-O bulk sample ($\sim -13\%$)³ in a field of the same strength.

Figure 7 shows a relationship between T_p and maximum $|\Delta R/R_0|$ in $\text{La}_{(2-x)/3}\text{Nd}_{x/3}\text{Ca}_{1/3}\text{MnO}_3$ bulk samples at a field of 0.67 T . $|\Delta R/R_0|_{\text{max}}$ increases linearly with the decrease of T_p . For $x=1.2$, $|\Delta R/R_0|$ is about 90% at 80 K in a field of 0.67 T , but its maximum value is not observed down to 77 K . For $x=1.5$ and 2 , the resistivity exhibits semiconducting behavior between 77 and 300 K in a field up to 0.67 T , and the MR effect is very small.

It is well known that the MR ratio in $R_{1-x}A_x\text{MnO}_3$ does not show a saturation even at much higher magnetic fields. At a higher applied field, $|\Delta R/R_0|_{\text{max}}$ will increase and the linear relationship between $|\Delta R/R_0|_{\text{max}}$ and T_p may be broken. However, the correlation between $|\Delta R/R_0|_{\text{max}}$ and T_p that $|\Delta R/R_0|_{\text{max}}$ increases with the decrease of T_p was still observed at a higher applied field.^{8,9}

IV. DISCUSSIONS

The XRD pattern reveals that at room temperature the crystal structure of $\text{La}_{(2-x)/3}\text{Nd}_{x/3}\text{Ca}_{1/3}\text{MnO}_3$ belongs to an orthorhombically distorted perovskite structure. For an ideal perovskite structure (ABO_3), the crystal symmetry imposes a strong constraint on the ratio of A-O and B-O bond lengths: $d_{A-O}/d_{B-O} = \sqrt{2}$ (i.e., tolerance factor $t=1$). If the atom A is too large for the cubic cage (BO_3), the cage is in tension and the atom A in compression ($t > 1$). If atom A is too small, the situation is reversed ($t < 1$). Therefore, some internal stress will be introduced in the structure when there exists a size mismatch between atoms at A site and B site. The internal stress can be partially relieved by structure distortion. The cubic structure is distorted either by the atom

TABLE II. Bond valence sum around each cation (V_i) and average bond valence sum around each cation site.

Composition	0.00	0.15	0.30	0.45	0.60	0.75	1.00	1.20	1.50	2.00
$V_{La^{3+}}$	3.09	3.13	3.15	3.14	3.21	3.22	3.25	3.31	3.37	
$V_{Nd^{3+}}$		2.61	2.63	2.62	2.68	2.69	2.71	2.76	2.82	2.91
$V_{Ca^{2+}}$	1.77	1.80	1.81	1.80	1.84	1.85	1.87	1.90	1.94	2.01
\bar{V}_R	2.65	2.66	2.65	2.62	2.65	2.63	2.61	2.62	2.62	2.61
$V_{Mn^{3+}}$	3.58	3.56	3.57	3.58	3.55	3.56	3.55	3.56	3.53	3.51
$V_{Mn^{4+}}$	3.51	3.50	3.50	3.51	3.49	3.49	3.49	3.49	3.46	3.44
\bar{V}_{Mn}	3.55	3.54	3.54	3.55	3.53	3.54	3.53	3.53	3.51	3.49

B moving off center in its octahedron (when atom A is too large) giving rise to a ferroelectric phase (e.g., $BaTiO_3$) or by the cage collapsing by a rotation of the octahedra (when atom A is too small) leading to a ferroelastic phase. In both cases the environment of the cation that is in tension is distorted, which gives rise to a bending of B -O- B bond.¹⁴

Bond valence sum of an atom can be used to examine the internal stress around the atom.^{14,15} The valence of a bond is defined as

$$s = \exp\left(\frac{R_0 - R}{B}\right)$$

where $B = 0.37 \text{ \AA}$, R is the bond length in \AA and R_0 is the bond length of unit valence. In general, the sum of the valences of the bonds formed by any atom, V , is equal to its atomic valence (valence-sum rule). The valence sum rule will be violated if there exists internal stress in the structure. If the bond valence sum of an atom V is larger than its atomic valence, the atom is in compression, and if V is smaller than its atomic valence, the atom is in tension. From the measured lattice parameters (Fig. 2) and the atomic parameters (Table I), the bond valence sum around each cation and the average bond valence sum around each cation site in $La_{(2-x)/3}Nd_{x/3}Ca_{1/3}MnO_3$ are calculated and listed in Table II. The values of R_0 for La^{3+} , Nd^{3+} , Ca^{2+} , Mn^{3+} , and Mn^{4+} are 2.172, 2.105, 1.967, 1.760, and 1.753, respectively.¹⁶ The average bond valence sum around R site, \bar{V}_R , is smaller than the expected average atomic valence (2.67), and that around Mn site \bar{V}_{Mn} is larger than the expected value (3.33). In other words, on average the ions at R site are in tension, while Mn ions are in compression, and thus the structure is distorted mainly by rotations of MnO_6 octahedra. The deviation of the calculated bond valence sums from the expected values is indicative of an incomplete release of the internal stress by structure distortion. However, the bond valence sum around each cation at R site indicates that La^{3+} is in compression, while Nd^{3+} and Ca^{2+} are in tension. Therefore, local lattice distortions around La^{3+} ions are different from those around Nd^{3+} and Ca^{2+} ions. The MnO_6 octahedra around Nd^{3+} and Ca^{2+} are likely to rotate to relieve the internal stress, which will lead to a larger bending of Mn-O-Mn bond. As shown in Table I, the angles of Mn-O-Mn bonds decrease with the increase of Nd content, and accordingly the distortion ratio D increases (Fig. 2). The

existence of inhomogeneous local distortion of the lattice might lead to a complex magnetic structure of the compounds.

In an ideal cubic perovskite $RMnO_3$, the anion $p\sigma$ orbitals are orthogonal to the t_{2g} orbitals of Mn ions and the anion $p\pi$ orbitals orthogonal to e_g orbitals. The deformation and rotation of MnO_6 octahedra can disturb the orthogonality of the orbitals and in general result in an occurrence of antiferromagnetic (AFM) superexchange interaction between Mn ions, which will compete with the ferromagnetic (FM) interaction.^{11,13,17} According to de Gennes,¹⁸ the competition of the coexisting AFM and double-exchange interactions between Mn ions always leads to a distortion of the ground-state spin arrangement and thus gives rise to a canted spin structure, since the electron transfer lowers the energy by a term of first order in the distortion, while the initial exchange energy is increased only in second order. The canted spin structure can be stable up to a well-defined temperature T_1 , and above T_1 the system can be antiferromagnetic, ferromagnetic, or paramagnetic, depending upon the relative amount of mobile electrons. Taking into account a low spontaneous magnetization at 77 K,¹¹ a larger distortion ratio D (Fig. 2) and semiconducting resistivity between 77 and 300 K (Fig. 6) of $Nd_{2/3}Ca_{1/3}MnO_3$, its magnetic structure at low temperature is likely to be a canted spin structure.

As shown in Figs. 3–5, the magnetization of the low moment state at high temperature increases with the increase of La content in $La_{(2-x)/3}Nd_{x/3}Ca_{1/3}MnO_3$. For the sample with $x = 0.75$, the magnetization of the low moment state at 0.5 T could be as high as $\sim 60 \text{ emu/g}$ ($\sim 2.26 \mu_B/\text{Mn}$), indicating that the low moment state at high temperature cannot be an antiferromagnetic one. An alternative possibility is that the low moment state corresponds to a canted spin structure and transits to a collinear ferromagnetic state at low temperature, which, however, is inconsistent with de Gennes' prediction. In addition, the magnetic transition temperature at low temperature for $x = 0.75$ –1.0 lies on the extrapolation line (dashed line in Fig. 4) of the Nd-rich branch of the T_m - x curve, while the magnetic transition temperature at high temperature for $x = 0.75$ –1 is consistent with the La-rich branch of the T_m - x curve. Therefore, the low moment state at high temperature and the high moment state at low temperature in $La_{(2-x)/3}Nd_{x/3}Ca_{1/3}MnO_3$ (Fig. 5) seem to be associated with the magnetic structures of end compounds $La_{2/3}Ca_{1/3}MnO_3$ and $Nd_{2/3}Ca_{1/3}MnO_3$, respectively.

Based upon the structure refinement results and analysis of bond valence sum around each cation, it is reasonable to

expect an existence of magnetic inhomogeneity, i.e., simultaneous occurrence of ferromagnetic domains and nonferromagnetic domains, in $\text{La}_{(2-x)/3}\text{Nd}_{x/3}\text{Ca}_{1/3}\text{MnO}_3$. The magnetic inhomogeneity could originate from different local distortion of the lattice around La^{3+} and Nd^{3+} ions, since in the crystal structure of $\text{La}_{(2-x)/3}\text{Nd}_{x/3}\text{Ca}_{1/3}\text{MnO}_3$ compounds Nd^{3+} ions are in tension and the local lattice distortions around Nd^{3+} ions are mainly caused by the rotation of MnO_6 octahedra, while La^{3+} ions are in compression and the local lattice distortions around La^{3+} ions are different from those around Nd^{3+} ions. Taking into account that the end compounds $\text{La}_{2/3}\text{Ca}_{1/3}\text{MnO}_3$ and $\text{Nd}_{1/3}\text{Ca}_{1/3}\text{MnO}_3$ are ferromagnetic and nonferromagnetic, respectively, the inhomogeneous local lattice distortions might give rise to a simultaneous occurrence of metallic La-rich ferromagnetic domains and semiconducting Nd-rich domains. Then the magnetization of the low moment state at high temperature shown in Figs. 3 and 5 could be attributed to the La-rich phase. As the La content increases, the volume fraction of La-rich phase increases, and the magnetization of the low moment state at high temperature increases accordingly. The Nd-rich phase is expected to transit to a canted spin structure at low temperature, which might be responsible for the second magnetic transition observed in compounds with $x=0.75$ and 1.0 (Fig. 5). At a higher applied field, the magnetization curve becomes a unified one corresponding to an almost fully spin-polarized state, which is indicative of the occurrence of a field-induced magnetic transition. The field-induced magnetic transition is evident in magnetization isotherms shown in the inset in Fig. 5. Based on the magnetic inhomogeneity model, the low moment plateau in the isotherms sets in at nearly the same field for different temperatures and seems to correspond to the saturation of the La-rich phase,¹⁹ while the field-induced magnetic transition occurs in the Nd-rich phase, the onset field of which decreases with decreasing temperature. For the sample with $x=1.2$, the low moment state at high temperature is hardly detected at a field of 0.5 T, but its magnetization curve is also switched to the one corresponding to an almost fully spin-polarized state at a field of 5 T (Fig. 5). For the end compound $\text{Nd}_{2/3}\text{Ca}_{1/3}\text{MnO}_3$, however, neither the field-induced magnetic transition nor the saturation is observed at 50 K in the fields up to 6.5 T. These observations seem to indicate that the coexisting La-rich phase might have an induction effect on the field-induced magnetic transition in Nd-rich phase.

Within the framework of the magnetic inhomogeneity model, the coexisting La-rich domains and Nd-rich domains are assumed to distribute randomly in the compound. In zero field, the La-rich ferromagnetic domain is metallic ($d\rho/dT > 0$) below T_c , and the Nd-rich domain is semiconducting ($d\rho/dT < 0$) between 77 and 300 K. Therefore, the resistivity peak could result from opposite temperature dependence of resistivity in La-rich domains and Nd-rich domains. As the La content increases, the volume fraction of La-rich phase increases, and the contribution of metallic conductivity to the conductivity of the compound increases, which will result in a shift of the resistivity peak to a higher temperature as shown in Figs. 4 and 6. Based upon the magnetic inhomogeneity model, the peak position of resistivity does not necessarily correspond to a magnetic transition temperature as observed in many $R_{1-x}A_x\text{MnO}_3$ compounds⁸

and confirmed by neutron diffraction experiment,²⁰ but depends on the relative contribution of metallic phase and insulating phase to the resistivity of the compound. The larger the contribution of metallic phase is, the higher the peak temperature. Taking peak temperature of resistivity as a magnetic transition temperature as in Ref. 9 is, in our opinion, an approximation exclusively for the $R_{1-x}A_x\text{MnO}_3$ compounds with an almost fully spin-polarized magnetic moment as shown in Fig. 4.

As shown in the inset in Fig. 5, a low applied field ($H < 1$ T) essentially increases the magnetization drastically of the La-rich ferromagnetic phase,¹⁹ corresponding to an initial magnetization process before saturation, and reduces the resistivity of the La-rich phase accordingly, which will give rise to a shift of the resistivity peak to a higher temperature and a large magnetoresistance effect. An applied field affects the conductivity of the compound most effectively at the temperature range where the contributions of the La-rich phase and Nd-rich phase are comparable. Therefore, a prominent MR effect occurs around the resistivity peak of $\rho(0) - T$. At a higher applied field ($H > 1$ T), the magnetization of the La-rich phase approaches to saturation, while the Nd-rich phase might undergo a field-induced magnetic transition, and the MR ratio could be further increased.

V. SUMMARY

The crystal structure, ac susceptibility, magnetization, and magnetoresistance behavior of $\text{La}_{(2-x)/3}\text{Nd}_{x/3}\text{Ca}_{1/3}\text{MnO}_3$ are investigated. Crystal structure refinement results reveal that $\text{La}_{(2-x)/3}\text{Nd}_{x/3}\text{Ca}_{1/3}\text{MnO}_3$ compounds crystallize in an orthorhombically distorted perovskite structure (O' -structure) at room temperature. As the Nd content increases, the lattice distortion and the bending of Mn-O-Mn bond increase. The local lattice distortions are discussed based on crystal structure refinement results and bond valence theory.

Low field ac susceptibility measurements between 77 and 300 K show that the magnetic transition temperature decreases with the increase of Nd content. For $x=0.75-1$, two magnetic transition temperatures are observed, and the magnetic transition at high temperature seems to be related to that of $\text{La}_{2/3}\text{Ca}_{1/3}\text{MnO}_3$, while magnetic transition at low temperature is related to that of $\text{Nd}_{2/3}\text{Ca}_{1/3}\text{MnO}_3$. The magnetization curve becomes a unified one corresponding to an almost fully spin-polarized state at higher fields. The magnetization isotherms reveal a field-induced magnetic transition in the sample.

Resistivity and magnetoresistance of bulk sample are measured between 77 and 300 K. For $x \leq 1.2$, a resistivity peak is observed in zero field and larger magnetoresistance occurs around the resistivity peak. In bulk $\text{La}_{1/3}\text{Nd}_{1/3}\text{Ca}_{1/3}\text{MnO}_3$ sample, a MR ratio as high as -96% is achieved in a low field of 0.67 T, which is much larger than previous reports on bulk $R_{1-x}A_x\text{MnO}_3$ in a field of the same strength. In addition, a linear dependence of maximum MR ratio in a field of 0.67 T on the peak temperature of resistivity in zero field is observed.

Based upon the discussion on local lattice distortion and measurements of ac susceptibility, magnetization, and resistivity, a magnetic inhomogeneity model, i.e., simultaneous

occurrence of metallic La-rich ferromagnetic domains and semiconducting Nd-rich domains, is proposed for the magnetic structure of $\text{La}_{(2-x)/3}\text{Nd}_{x/3}\text{Ca}_{1/3}\text{MnO}_3$. It is argued that the magnetic inhomogeneity could originate from the different local distortions of lattice around La^{3+} and Nd^{3+} ions. Within the framework of the magnetic inhomogeneity model, the occurrence of resistivity peak could result from a competition of opposite temperature dependence of resistivity in La-rich phase and in Nd-rich phase and thus the peak temperature does not necessarily correspond to a magnetic transition temperature. The low-field giant magnetoresis-

tance effect might be associated with the initial magnetization process of the La-rich phase at low field. A field-induced magnetic transition occurs in the Nd-rich phase. The coexisting La-rich phase seems to have an induction effect on the field-induced magnetic transition.

ACKNOWLEDGMENTS

This work was supported by National Natural Science Foundation of China. The authors would like to thank X.R. Cheng for his assistance in experiments.

-
- ¹S. Jin, T.H. Tiefel, M. McCormack, P.A. Fastnacht, R. Ramesh, and L.H. Chen, *Science* **264**, 413 (1994).
²G.C. Xiong, Q. Li, H.L. Ju, S.N. Mao, L. Sanapati, X.X. Xi, R.L. Greene, and T. Venkatesam, *Appl. Phys. Lett.* **66**, 1427 (1995).
³S. Jin, H.M. O'Bryan, T.H. Tiefel, M. McCormack, and W.W. Rhodes, *Appl. Phys. Lett.* **66**, 382 (1995).
⁴G.Q. Gong, C.C. Canedy, G. Xiao, J.Z. Sun, A. Gupta, and W.J. Gallagher, *Appl. Phys. Lett.* **67**, 1783 (1995).
⁵A. Maignan, Ch. Simon, V. Caignaert, and B. Raveau, *Solid State Commun.* **96**, 623 (1995).
⁶Y. Tokura, A. Urushibara, Y. Moritomo, T. Arima, A. Asamitsu, G. Kido, and N. Furukawa, *J. Phys. Soc. Jpn.* **63**, 3931 (1994).
⁷C. Zener, *Phys. Rev.* **82**, 403 (1951).
⁸H.Y. Hwang, S.-W. Cheong, P.G. Radaeli, M. Marezio, and B. Batlogg, *Phys. Rev. Lett.* **75**, 914 (1995).
⁹J. Fonteberta, B. Martínez, A. Seffar, S. Piñol, J.L. García-Muñoz, and X. Obradors, *Phys. Rev. Lett.* **76**, 1122 (1996).
¹⁰E.O. Wollan and W.C. Koehler, *Phys. Rev.* **100**, 545 (1955).
¹¹V.A. Bokov, N.A. Grigorgan, M.F. Bryzhina, and V.V. Tikhonov, *Phys. Status Solidi* **28**, 835 (1968).
¹²D.B. Wiles and R.A. Young, *J. Appl. Cryst.* **14**, 149 (1981).
¹³Z. Jiráček, S. Krupica, Z. Simsa, M. Dlouhá, and S. Vratislav, *J. Magn. Magn. Mater.* **53**, 153 (1985).
¹⁴I.D. Brown, *Acta Crystallogr. B* **48**, 553 (1992).
¹⁵I.D. Brown, *J. Solid State Chem.* **90**, 155 (1991).
¹⁶I.D. Brown and D. Altermatt, *Acta Crystallogr. B* **41**, 244 (1985).
¹⁷E. Pollert, S. Krupicka, and E. Kuzmiciva, *J. Phys. Chem. Solids* **43**, 1137 (1982).
¹⁸P.G. de Gennes, *Phys. Rev.* **118**, 141 (1960).
¹⁹H.L. Ju, J. Gopalakrishnan, J.L. Peng, Q. Li, Q.C. Xiong, T. Venkatesan, and R.L. Greene, *Phys. Rev. B* **51**, 6143 (1995).
²⁰D.N. Argyriou, J.F. Mitchell, C.D. Potter, D.G. Hinks, J.D. Jorgensen, and S.D. Bader, *Phys. Rev. Lett.* **76**, 3826 (1996).